

Spatially correlated distributions of local metallic properties in bulk and nanocrystalline GaNJames P. Yesinowski,^{1,*} Zachariah J. Berkson,² Sylvian Cadars,³ Andrew P. Purdy,¹ and Bradley F. Chmelka²¹*Chemistry Division, Naval Research Laboratory, Washington DC 20375-5342, USA*²*Department of Chemical Engineering, University of California, Santa Barbara California 93106-5080, USA*³*Institut des Matériaux Jean Rouxel, Université de Nantes, CNRS, BP32229, F-44322 Nantes Cedex 3, France*

(Received 5 July 2016; published 9 June 2017)

We compare local electronic structure at different atom types of a metallic semiconductor in bulk and nanocrystalline form. Multinuclear magic-angle-spinning nuclear magnetic resonance (MAS NMR) establishes that GaN synthesized as an intentionally doped bulk powder or as annealed nanocrystalline particles exhibits metallic behavior and a wide distribution of differing electronic environments in both forms. Bulk polycrystalline wurtzite GaN doped with 0.13% Ge as a shallow donor exhibits a temperature-independent distribution of ^{71}Ga Knight shifts over the temperature range 123–473 K. Each Knight shift frequency in the inhomogeneously broadened spectrum is characterized by a ^{71}Ga spin-lattice relaxation time T_1 that is in good agreement with the value predicted by the Knight-Korringa relation across the broad range of temperatures. The ^{14}N spectrum shows a slightly smaller Knight shift distribution with spin-lattice relaxation time T_1 values at 295 K across the distribution also in good agreement with the Knight-Korringa relation. Similarly, annealed nanocrystalline wurtzite GaN (50–100 nm, and without Ge) exhibits a ^{71}Ga Knight shift distribution and T_1 values (at 295 K) that follow the same Knight-Korringa behavior. Thus, both bulk and nanocrystalline forms of GaN are n type and well above the metal-insulator transition (MIT), the nanocrystals most likely as a result of incorporation of shallow donor oxygen atoms during synthesis. Carriers in both forms of samples exhibit the near-ideal characteristics of a degenerate Fermi gas of noninteracting spins. The observation of NMR signals from both atom types, Ga and N, allows for the direct spatial correlation of the local electronic structure at the two sites in the lattice, specifically the *s*-orbital character of the electronic wave function of conduction band electrons at the Fermi edge. The relative values of these carrier wave-function probabilities (nearly twice as great for the N atom as for the Ga) are in line with theoretical predictions. Analyses of ^{71}Ga , ^{14}N , and ^{15}N NMR results, including double-resonance 2D $^{15}\text{N}\{^{71}\text{Ga}\}$ measurements, reveal electronic disorder in the form of broad distributions of local metallic properties (Knight shifts) that are shown to be spatially correlated on a subnanometer scale.

DOI: [10.1103/PhysRevB.95.235201](https://doi.org/10.1103/PhysRevB.95.235201)**I. INTRODUCTION**

Semiconductors heavily doped with shallow donors become metallic, acquiring useful electronic and photonic properties. Mott provided a quantitative estimate of the donor concentration required to induce such a transition [1], known as the metal-insulator transition (MIT) or Mott transition. Physically, this corresponds to a transition between two extrema: (1) dilute isolated and independent shallow donors, that at low temperatures are un-ionized and have weakly bound electrons whose wave functions [2] typically extend over several lattice constants; and (2) concentrated and interacting shallow donors, whose overlapping wave functions form an impurity band that can lie below the conduction band or, at higher concentrations, enter into it. Magnetic resonance techniques based upon observing either the electron spin, e.g., electron paramagnetic resonance (EPR) or the nuclear spin via the electron spin, e.g., electron-nuclear double resonance (ENDOR) have provided very detailed insights on local electronic structures in the first regime [3–6], but not the second. Detailed experimental and theoretical understanding of the spatially varying electronic structures of heavily doped semiconductors is challenging because of the electronic disorder arising from the assumed random substitutions of shallow donors in the lattice [7].

One of the few means of observing such electronic disorder over the atomic scale is provided by magnetic resonance

techniques that exploit well-understood interactions between electron and nuclear spins. Extensive magnetic resonance studies on doped Si around the MIT, including nuclear magnetic resonance (NMR) studies [7–14], have yielded important insights into local electronic structure. However, an unambiguous interpretation of the NMR results has proven difficult because of complications due to formation of impurity bands distinct from the conduction band [12,13]. Furthermore, no direct experimental evidence has yet been obtained for spatial variations in the electronic structure about individual silicon atoms in metallic doped samples.

By working with the compound semiconductor hexagonal (or wurtzite) gallium nitride (h-GaN), which has technologically important applications in solid-state lighting and power electronics [15,16], we have directly correlated spatial variations in the electronic structures of constituent atoms in semiconductor samples well above the MIT. The insights come from two main sources. There are frequency displacements, called Knight shifts (K), of the ^{71}Ga , ^{14}N , and ^{15}N NMR signals that arise here from nuclear hyperfine interactions with electrons in the conduction band having *s*-orbital character [17]. There are also associated contributions to the overall spin-lattice relaxation rate T_1^{-1} from the Korringa relaxation term $T_{1,K}^{-1}$ [17].

In this work we show that both bulk polycrystalline GaN prepared from an alkali-metal flux containing Ga and Ge under N_2 pressure and containing 0.13 wt% Ge as a substitutional n-type dopant (GaN:Ge) [18,19], as well as

*yesinowski@nrl.navy.mil

annealed nanocrystalline GaN powders, are highly metallic, i.e. are well above the MIT. Our results resolve widely differing interpretations of the electronic structure of nanocrystalline GaN powders manifested by their ^{69}Ga , ^{71}Ga , and ^{15}N NMR spectra [14,20–26]. The results also represent a detailed electronic structural characterization of a degenerately doped semiconductor in bulk and nanocrystalline forms. While both GaN:Ge and nanocrystalline GaN materials exhibit properties that are characteristic of degenerate Fermi gases of noninteracting spins, the local metallic properties, as reflected by the Knight shifts and Korringa relaxation rates, vary widely over subnanometer length scales. We determine the ratio of s -orbital carrier wave-function probabilities at the Fermi edge, with the N atoms having significantly more s character than the Ga atoms regardless of the local metallic property. Furthermore, the spatial correlation of local metallic properties at different neighboring spin pairs (in this case ^{71}Ga and ^{14}N or ^{15}N) provides a strong indication that the Knight shift distributions are due to electronic disorder related to the proximities to randomly located shallow donors.

II. RESULTS AND DISCUSSION

A. Bulk GaN:Ge powder

1. ^{71}Ga and ^{14}N Knight shifts

Both ^{71}Ga and ^{14}N magic-angle spinning (MAS) NMR spectra of GaN:Ge show broad Knight-shifted signals arising from distributions of ^{71}Ga and ^{14}N electronic environments. Figure 1(a) shows the central transitions ($+1/2$ to $-1/2$) of six overlaid ^{71}Ga spectra acquired at temperatures from 123 to 473 K. The small narrow peak at ca. 332 ppm corresponds to undoped h-GaN [27] and is assigned to regions of the sample that experience no Knight shift. A magnification of this region for the spectra collected at all six temperatures is shown in Fig. 2(a). The considerably broader ^{71}Ga signals dominating the spectra arise from regions of the sample having different Knight shifts [18]. Unlike doped Si above the MIT [28], the distribution of Knight-shifted intensity is essentially temperature independent, as discussed below.

Figure 2(b) shows that the chemical shift of the zero Knight shift peak has a weak dependence upon temperature, varying linearly with T^2 . This likely reflects the quadratic temperature dependence of the hexagonal GaN lattice parameters [29]. When this temperature dependence is taken into account in referencing the ^{71}Ga Knight shift distributions to the position of this particular peak maximum at each temperature, the Knight shifts are clearly independent of temperature. This is shown by the comparison of the same region on the left edge of the broad ^{71}Ga peaks before [Fig. 2(c)] and after [Fig. 2(d)] application of the temperature-dependent correction.

We use this temperature independence of the Knight shift K over the temperature range 123–473 K to estimate a lower bound for the Fermi level in GaN:Ge. We use Eq. (5) of Ref. 13, rewritten below, to obtain the factor (in square brackets) involving $(T/T_F)^2$ that scales the Knight shift at different temperatures T depending upon the value of the Fermi temperature T_F , for the situation where $T < T_F$:

$$K = 2\pi \left(\frac{\gamma_s^2 \hbar^2}{2} \right) \left(\frac{P_f}{k_B T_F} \right) \left[1 - \frac{\pi^2}{12} \left(\frac{T}{T_F} \right)^2 \right]. \quad (1)$$

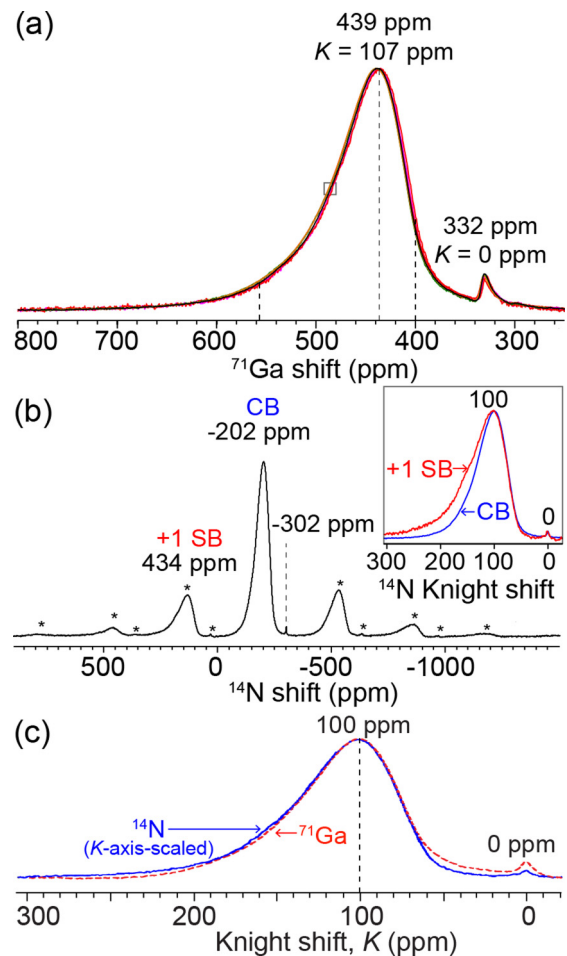


FIG. 1. MAS-NMR spectra of bulk GaN:Ge powder at 11.7 T. (a) Overlaid ^{71}Ga spectra (5-kHz MAS, 15-s delay) at different temperatures from 123 to 473 K; see Figs. 2(a) and 2(c) for expanded views of the peak at $K=0$ and the left edge region indicated by the small box; (b) ^{14}N rotor-synchronized Hahn-echo NMR spectrum (12-kHz MAS, 20-s delay) acquired at 295 K. Spinning sidebands (SB) are indicated by asterisks. (c) Comparison of the Knight shift distributions of ^{71}Ga and ^{14}N (obtained by summing the CB and three pairs of SBs), with normalized peak heights and with an x axis corresponding to the ^{71}Ga Knight shift and the ^{14}N Knight shift scaled by a factor of 1.059 to give the best overlap.

Here γ_s is the electron gyromagnetic ratio, \hbar is Planck's constant, and P_f is a measure of the average electronic probability density at the nucleus; we assume that the derivation of this equation applied to ^{31}P in Si:P is valid for ^{71}Ga in GaN. Assuming a T_F of 4500 K yields a scaling factor of 0.991 at 473 K and 0.999 at 123 K, the two extremes of temperature. The 0.008 difference in the scaling factors would result in a 1.2-ppm change in the Knight shifts at the 155-ppm edge shown in Fig. 2(d). Since any actual change in the Knight shift with temperature must be smaller than the measurement uncertainty, ca. 1.2 ppm, we conclude that T_F is greater than 4500 K, which corresponds to a Fermi energy of ca. 400 meV above the bottom of the conduction band. Thus, the GaN:Ge doping is extremely degenerate ($T_F/T > 10$) over the range of temperatures investigated, in agreement with further evidence from relaxation analyses below. A Fermi level at least 400 meV above the bottom of the conduction band is plausible, since

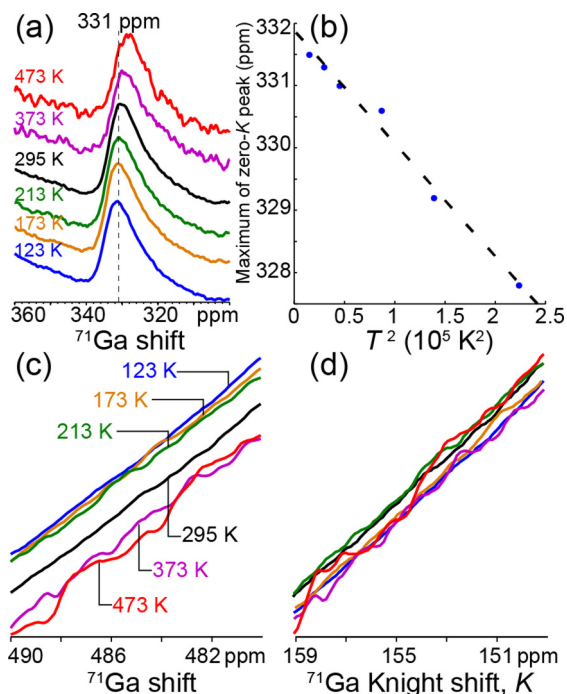


FIG. 2. (a) ^{71}Ga MAS NMR spectra of GaN:Ge at different indicated temperatures, showing an enlargement of the zero-Knight shift peak region for the spectra shown in Fig. 1(a). The six spectra are offset for clarity. (b) Plot of the peak position of the zero-Knight shift peak as a function of T^2 . The dotted line has a slope of -1.81×10^{-5} ppm/K 2 and represents a linear best fit to the data points. (c) ^{71}Ga MAS NMR spectra of GaN:Ge at different indicated temperatures, showing the temperature dependence of a high-frequency region of the spectra. (d) The same high-frequency region as (c), with the x axis rescaled such that the maximum of the zero-Knight shift peak shown in (a) has a shift of 0 ppm at each temperature. After correction for the small temperature dependence of the zero-Knight shift peak, the ^{71}Ga Knight shift is thus shown to be temperature independent across the inhomogeneously broadened spectrum shown in Fig. 1(a).

DFT calculations for GaN doped with a carrier concentration of 1×10^{19} cm $^{-3}$ give a Fermi level of 125 meV above the conduction band minimum [30], whereas the GaN:Ge sample is estimated to have a carrier concentration in the range $0.7 - 1.8 \times 10^{20}$ cm $^{-3}$ [18]. These estimated values are well above the MIT for n-type GaN:Si of 1.6×10^{18} cm $^{-3}$ [31] and theoretical predictions for h-GaN of 1×10^{18} cm $^{-3}$ [32].

The ^{14}N spectrum of GaN:Ge in Fig. 1(b) corroborates and extends these conclusions. It has a centerband region showing a weak narrow signal at -302 ppm, the same shift as observed for undoped h-GaN [27]. A dominant inhomogeneously broadened peak is also present at -202 ppm, reflecting a distribution of Knight shifts. In addition to the centerband, a set of spinning sidebands spaced at integer multiples of the spinning rate (12 kHz) reflect the ^{14}N nuclear quadrupole coupling constant (NQCC) arising from (first-order) interactions between the nuclear electric quadrupole moments and the electric field gradients at the nuclei. The NQCC is axially symmetric (asymmetry parameter $\eta = 0$), with a quadrupole coupling constant C_q ($=e^2Qq/h$) of 24.14 kHz at 296 K [33].

The inset in Fig. 1(b) shows a region centered on the $+1$ sideband superimposed upon an equivalent region of the centerband and normalized to the same peak height. The greater intensity on the left side of the sideband spectrum indicates that those regions of GaN:Ge having larger Knight shifts also have significantly altered anisotropic interactions that cause their sideband intensities to increase relative to the centerband. In principle these altered interactions could result from changes in the electric field gradients at the ^{14}N sites that change the NQCC or from an increase in the ^{14}N chemical shift anisotropy from its value of zero in an undoped GaN film [33]. Although the latter cause seems less likely, the corresponding increase in intensity of Knight-shifted regions seen for the -1 sideband is somewhat less than that for the $+1$ sideband, an asymmetric behavior that is not expected for alterations of the NQCC alone. This correlation between the charge (NQCC, or possibly chemical shift as well) and the spin (Knight shift) effects of dopants has been seen in ^{71}Ga spectra of GaN films [34] and suggests that the most Knight-shifted ^{14}N and ^{71}Ga nuclei are closest to the dopants.

Complementary analyses of the ^{71}Ga and ^{14}N Knight-shift distributions directly relate the conduction electron density at Ga and N lattice sites. The Knight shift K due to the contact interaction in a Fermi gas of noninteracting electron spins, after replacing the spin contribution to the susceptibility χ_e^s by $\gamma_e^2 \hbar^2 \rho_0(E_F)/2$, is described by [17]

$$K = \frac{4\pi}{3} \gamma_e^2 \hbar^2 \langle |u_k(0)|^2 \rangle_{E_f} \rho_0(E_f). \quad (2)$$

Here, $\langle |u_k(0)|^2 \rangle_{E_f}$ is the probability of an electron at the Fermi level in an s orbital being at the nucleus, $\rho_0(E_f)$ is the density of states (DOS) of this s orbital at the Fermi level, γ_e is the electron gyromagnetic ratio, and \hbar is Planck's constant. Interestingly, after scaling the ^{14}N frequency axis by a factor of 1.059, the shapes of the ^{71}Ga and ^{14}N intensity distributions are nearly identical [Fig. 1(c)]. This suggests that each ^{71}Ga nucleus associated with a particular ^{71}Ga Knight shift isochromat has neighboring ^{14}N nuclei with correlated Knight shifts. The scaling factor provides a direct experimental means of comparing, at both atomic sites, the relative s -orbital characters of the conduction band electrons at the Fermi edge.

2. Comparison of electronic projected densities of states at ^{71}Ga and ^{14}N lattice sites

The probability $\langle |u_k(0)|^2 \rangle_{E_f}$ for electron wave functions at Ga and N atoms can be estimated from theoretical calculations of atomic hyperfine coupling constants of atoms [35], parameters of great interest in EPR spectroscopy. For unit spin density, the probabilities of an s -orbital electron being at the nucleus for ^{14}N ($2s2p$ orbitals) and ^{69}Ga ($4s4p$ orbitals) are 5.60 a.u. $^{-3}$ and 10.18 a.u. $^{-3}$, respectively [35]. Since the electron wave functions for ^{69}Ga and ^{71}Ga atoms are the same, the ratio of the amplitudes of the s -orbital electron wave functions, $\langle |u_k(0)|^2 \rangle_{E_f}$, at ^{71}Ga to those at ^{14}N nuclear sites for unit spin density may be expected to approximate 1.82 ($=10.18/5.60$). If the density of states $\rho_0(E_F)$ for the atomic s orbitals of N and Ga were equal for all of the atoms whose nuclei experience varying Knight shifts across the distribution, the ratio of the widths of the ^{71}Ga and ^{14}N Knight shift

distributions would be 1.82. Since the actual scaling factor to match the ^{71}Ga spectrum with the ^{14}N spectrum is 1.059, we conclude that the conduction band electrons at N atoms in Ge-doped GaN have a factor of 1.7 ($=1.82/1.059$) more atomic s -orbital character than those at the Ga atoms at each site in the distribution.

This detailed information about electronic structure at the two types of atoms in GaN doped n type should be able to provide an experimental check of the accuracy of theoretical calculations of GaN electronic structure. Although there have been a number of such calculations, what is required is a projected partial density of states (PDOS) of the wave functions at the conduction band edge onto the s orbitals of the Ga and N atoms. One such local density-functional calculation on undoped h-GaN using the LMTO method in conjunction with the LDA approach has been carried out, and the results have been compared with experimental results from synchrotron x-ray emission and absorption spectra that yield information on the PDOS [36]. From the graphical presentation of the s states of Ga and N at the conduction band edge (or 400 meV higher) given in Fig. 1 of this reference, it appears that the N atoms have a ca. $1.0 - 1.1 \times$ greater PDOS than the Ga atoms. This factor is not exceedingly far from the $1.7 \times$ factor deduced from the Knight shift results. Exact quantitative agreement is not to be expected, since the symmetry-determined projections onto s states forming the basis of the DFT results, while approximating $4s$ (for Ga) and $2s$ (for N) orbitals, are likely not identical to the atomic s orbitals used to interpret the Knight shift results from hyperfine calculations. The absolute magnitude of the two PDOS is also eliminated as a concern, since it is the relative magnitudes at Ga and N sites that are being compared. We note that double-resonance EPR measurements of Overhauser shifts due to residual donors in h-GaN [37] provide information about the greater relative strength of the hyperfine interactions of an electron to ^{14}N relative to ^{69}Ga or ^{71}Ga nuclei (although the ratio given based on the Overhauser shifts can be questioned because of the neglect of the different magnetogyric ratios for the two nuclei). The hyperfine interactions reflect a spatial average over a donor hydrogenic $1s$ orbital, and thus cannot be directly compared to our results involving delocalized (metallic) conduction band electrons.

3. Korringa T_1 relaxation of ^{71}Ga and ^{14}N

Associated with Knight shifts is the Korringa spin-lattice relaxation time $T_{1,K}$, which for the Fermi gas of noninteracting electrons assumed in Eq. (2) is given by [17]

$$\frac{1}{T_{1,K}} = \left(\frac{\gamma_n}{\gamma_e} \right)^2 \frac{4\pi k_B T}{\hbar} K^2, \quad (3)$$

where k_B is Boltzmann's constant and γ_n is the nuclear gyromagnetic ratio. Figure 3 summarizes ^{71}Ga $T_{1,K}$ measurements on GaN:Ge over the temperature range 123–473 K. The inset to Fig. 3(a) depicts the two rate constants W_1 and W_2 characterizing the single- and double-quantum quadrupolar relaxation processes, respectively, and the single rate constant W characterizing the magnetic (Korringa) relaxation process. Since $W_1 \cong W_2$ in GaN [38], the single-exponential time constant T_1 obtained from fitting the saturation-recovery

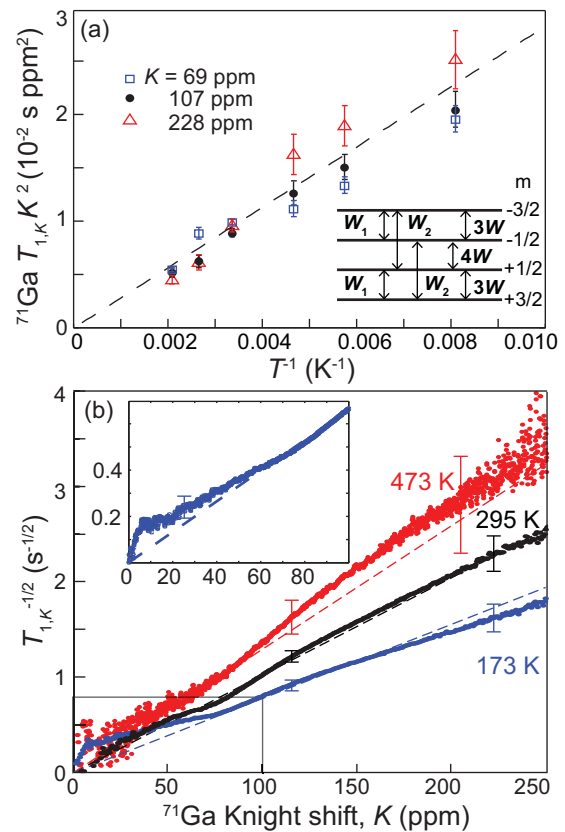


FIG. 3. Plots of ^{71}Ga MAS-NMR spin-lattice relaxation times due to Korringa relaxation $T_{1,K}$ for different temperatures and Knight shifts K in GaN:Ge. (a) $T_{1,K} K^2$ versus inverse temperature for three representative Knight-shifted signals indicated by dashed lines in Fig. 1(a). The dashed line is the theoretical prediction from Eq. (3). The inset shows transition rates between the ^{71}Ga ($I = 3/2$) Zeeman sublevels due to quadrupolar (W_1 and W_2) and magnetic (W) relaxation processes. (b) $T_{1,K}^{-1/2}$ plotted as a function of the ^{71}Ga Knight shift K at three temperatures; dashed lines are theoretical predictions from Eq. (3).

intensities (with complete saturation of all three transitions, a condition that was shown to be necessary to obtain physically meaningful ^{71}Ga relaxation results [26]) at each frequency in the spectrum obeys the equation [38] $1/T_1 = 2W_1 + 2W$. Thus, subtracting the quadrupolar relaxation term, measured at the zero-Knight shift peak, from the measured $1/T_1$ at any given frequency position in the spectrum yields $1/T_{1,K}$ ($= 2W$), the Korringa relaxation rate [18] (making the reasonable assumption that the quadrupolar relaxation term is constant across the Knight-shifted spectrum) [39]. By Eq. (3), this rate is proportional to K^2 , and $T_{1,K}$ is expected to depend linearly upon $1/T$ with a zero intercept for all K .

Using a reduced variable for the ordinate $T_{1,K} K^2$, we compare in Fig. 3(a) the relaxation data at six different temperatures from 123 to 473 K for three representative Knight shifts to a single theoretical dashed line obtained from Eq. (3). The linearity, slope, and zero intercept of the data for the various K values agree very well with the theoretical prediction, which involves no adjustable parameters. Temperature-dependent Korringa relaxation in n-type GaN has been observed, under conditions where a Knight shift

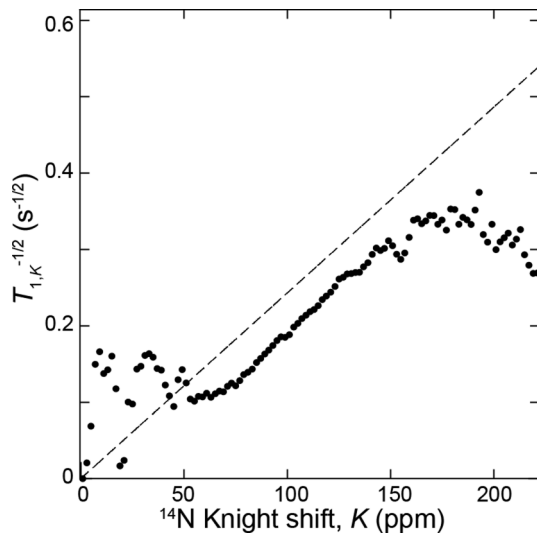


FIG. 4. Plot of ^{14}N $T_{1,K}^{-1/2}$ values as a function of the ^{14}N Knight shift K for bulk GaN:Ge. The dashed line is the theoretical prediction from Eq. (3). Spin-lattice relaxation times were measured at 295 K, 9 kHz MAS, and 11.7 T.

measurement was not possible [40]. Figure 3(b) shows the square root of these relaxation rates plotted against K for three representative temperatures, along with theoretical predictions based upon Eq. (3) (shown as dashed lines, and again involving no adjustable parameters). The deviations shown in the inset for small Knight shifts (<60 ppm) at low temperature (173 K) may represent the effects of freezing out and localization of donor electrons onto Ge sites, leading to more rapid relaxation at lower temperatures than predicted by the Korringa relation.

The ^{14}N Knight shifted signals in bulk GaN:Ge also exhibit Korringa relaxation. This is demonstrated by the Korringa relaxation plot for ^{14}N , shown in Fig. 4. The ^{14}N $T_{1,K}$ values were obtained by least-squares single-exponential fitting of saturation-recovery intensities at equally spaced intervals across the centerband region of the spectrum. The values for $T_{1,K}$ are obtained using Eq. (3) by setting $T_{1,0}$ to a value based on measurements of the peak at $K = 0$ (at -302 ppm). The agreement with the theoretical prediction for Korringa relaxation is reasonable. The systematic deviation from the theoretical prediction in the K range of 50–150 ppm, where fits are most reliable, is attributed to difficulties in properly removing the baseline contribution due to the overlap between the spinning sidebands and the centerband in the series of saturation recovery ^{14}N NMR spectra used to obtain the reported $T_{1,K}$ values.

B. Nanocrystalline GaN

1. ^{71}Ga Knight shifts and Korringa T_1 relaxation

The ^{71}Ga spectrum of nanocrystalline GaN in Fig. 5(b) exhibits similar evidence for distributions of local metallic environments. The sample (50- to 100-nm crystallite diameter by Scherrer analysis), produced by ammonolysis of GaO(OH) at 1100 °C with NH_3 , is crystalline h-GaN, as evidenced by the XRD pattern in Fig. 5(a). Similar ^{71}Ga spectral features as for bulk GaN:Ge are observed: a broad signal around 417 ppm and

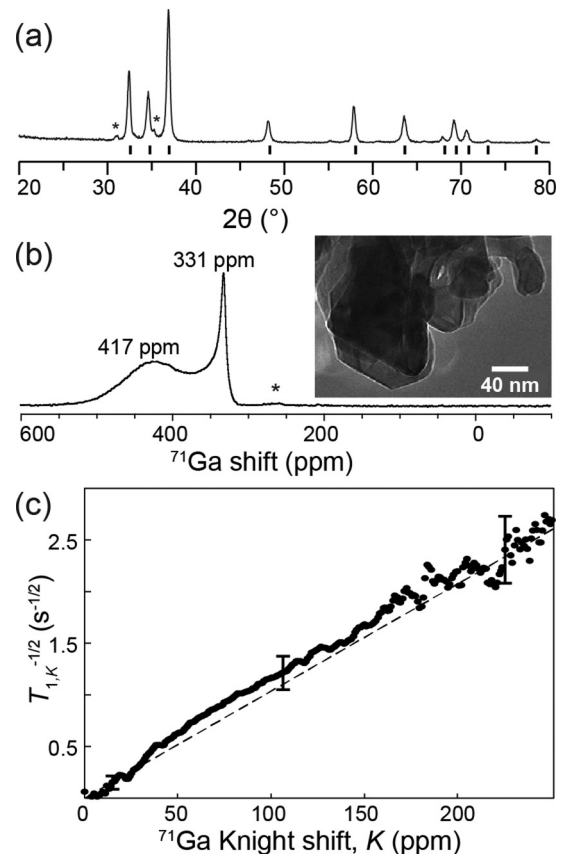


FIG. 5. (a) X-ray diffraction pattern of nanocrystalline GaN. The black lines indicate reflections indexable to wurtzite GaN (JCPDS Card No. 76-073); the asterisks indicate reflections indexable to $\beta\text{-Ga}_2\text{O}_3$ ($<3\%$, JCPDS Card No. 43-1012). (b) Rotor-synchronized ^{71}Ga MAS-NMR Hahn-echo spectrum (18 kHz MAS, 295 K, 18.8 T, 3-s delay) of nanocrystalline GaN; the inset shows a representative TEM image. (c) Plot of ^{71}Ga $T_{1,K}^{-1/2}$ values as a function of the ^{71}Ga Knight shift K ; the dashed line is the theoretical prediction from Eq. (3).

a narrow peak (11 ppm FWHM) at the shift position of undoped bulk h-GaN at 331 ppm [27]. The spin-lattice relaxation times obtained (using single-exponential fits) and analyzed as discussed above yield a plot of $(T_{1,K})^{-1/2}$ versus K , [Fig. 5(c)], in excellent agreement with the theoretical line from Eq. (3). Similar distributions of ^{71}Ga Knight shifts, but affecting a smaller proportion of Ga atoms, are observed for smaller-size GaN nanocrystals (8–11 nm) [22,23]. The ^{71}Ga NMR relaxation analyses establish conclusively that the nanocrystalline GaN is heavily doped above the MIT, and demonstrate that synthesis of nanocrystalline GaN by ammonolysis is an effective way to introduce electrically active dopants into a semiconductor nanomaterial, which can otherwise be difficult [41]. Such NMR techniques provide a promising tool for understanding heavily doped semiconductor nanomaterials, which have interesting plasmonic properties for optoelectronic applications [42] but for which bulk electrical characterization methods are often infeasible due to the difficulties associated with making electrical contacts.

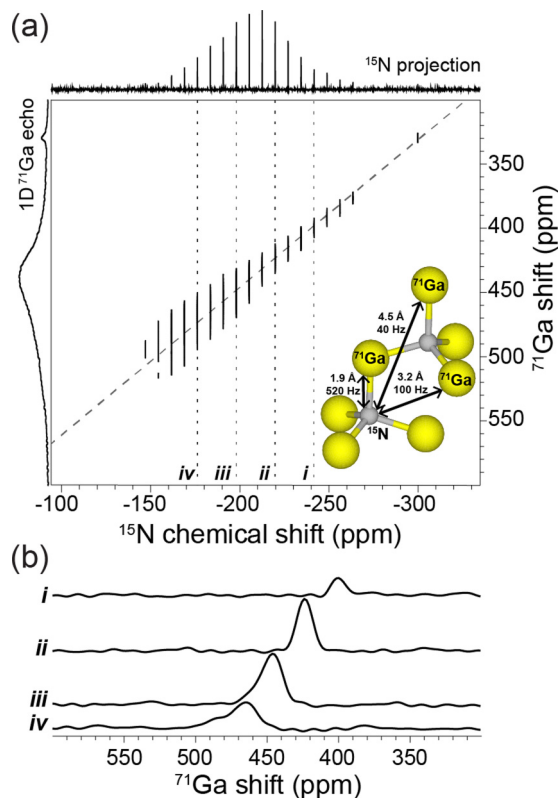


FIG. 6. (a) Two-dimensional $^{15}\text{N}\{^{71}\text{Ga}\}$ dipolar-mediated TEDOR correlation spectrum (20 kHz MAS, 298 K, 18.8 T) of ^{15}N -enriched GaN nanoparticles. A CPMG pulse sequence was used for detection to maximize the ^{15}N signal intensity [39], which yields a manifold of narrow peaks (spikelets) whose envelope reflects the ^{15}N shift distribution. A 1D ^{71}Ga echo spectrum is shown along the vertical axis for comparison. (b) Slices extracted from the 2D spectrum at positions indicated by the Roman numerals.

2. Two-dimensional NMR correlation of ^{71}Ga and ^{15}N Knight shifts

The ^{71}Ga and ^{15}N Knight shifts in nanocrystalline GaN are spatially correlated over atomic length scales. This is established by the 2D $^{15}\text{N}\{^{71}\text{Ga}\}$ transferred-echo double resonance (TEDOR) spectrum in Fig. 6 of a ^{15}N -labeled nanocrystalline GaN (Ga^{15}N) sample [39]. The TEDOR pulse sequence is useful for transferring polarization from one type of nucleus to another type via relatively weak dipolar couplings [43,44]. The two-dimensional version, which has been developed and applied to polarization transfer from quadrupolar nuclei to spin-1/2 nuclei [45–49], yields a 2D spectrum showing correlated signal intensity from spatially proximate nuclear spin pairs that are dipole-dipole coupled. In our case the result is a 2D contour plot with ^{71}Ga and ^{15}N shift axes (appearing severely compressed in the horizontal direction as a result of the spikelet character of the ^{15}N spectrum), and a 1D projection spectrum for ^{15}N . The relative intensity at each ^{15}N shift position reflects the number of ^{15}N nuclei at a given ^{15}N shift that are dipole-coupled (through space, <1 nm) to ^{71}Ga nuclei having the range of ^{71}Ga shifts depicted in the 2D contour plot. Perfectly correlated ^{71}Ga and ^{15}N shifts would yield a contour plot consisting of a narrow diagonal ridge, which resembles what is experimentally observed in Fig. 6(a).

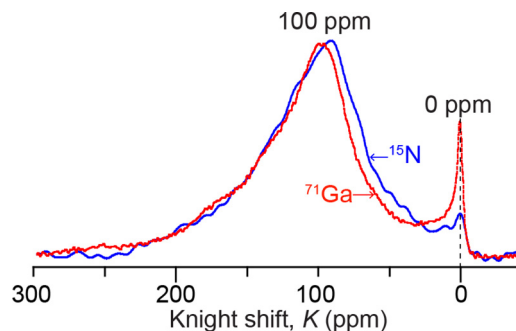


FIG. 7. Comparison of the Knight shift distributions of ^{71}Ga and ^{15}N for nanocrystalline Ga^{15}N , with normalized peak heights and with an x axis corresponding to the ^{71}Ga Knight shift and the ^{15}N Knight shift scaled by a factor of 1.052, the same as the slope of the dashed line in the TEDOR spectrum [Fig. 6(a)]. The ^{71}Ga spectrum (red) was acquired at 298 K, 18.8 T, 20 kHz MAS, and with a recycle delay of 10 s. The ^{15}N spectrum (blue) was acquired at 298 K, 7.4 T, and with a recycle delay of 240 s.

The slope of the best-fit diagonal in Fig. 6(a) is 1.052 ± 0.007 ($^{71}\text{Ga}/^{15}\text{N}$), the same (within experimental uncertainty) as the scaling factor of 1.059 ($^{71}\text{Ga}/^{14}\text{N}$) determined above for bulk GaN:Ge; Fig. 1(c). This equivalence for the two different approaches indicates that the relative s -orbital characters of the conduction band electrons at the Ga and N sites are very similar in bulk Ge-doped and nanocrystalline GaN. Representative vertical slices extracted from the TEDOR spectrum, Fig. 6(b), have widths that are considerably smaller than the overall 1D ^{71}Ga spectrum, again indicating that the respective ^{71}Ga and ^{15}N Knight shifts from neighboring atoms in the nanocrystals are correlated.

Figure 7 compares the shift distributions of ^{71}Ga and ^{15}N for the nanocrystalline Ga^{15}N sample, with the ppm axis for the latter scaled by the factor of 1.052 determined from fitting the TEDOR spectrum ridge, as described in the caption and text. As was the case with the analogous $^{71}\text{Ga}/^{14}\text{N}$ comparison for GaN:Ge shown in Fig. 1(c), the distributions are comparable in shape, although there is a slightly greater relative intensity for ^{15}N on the right side of the peak maxima.

It is noticeable in Fig. 6 that there is an increasing spread in the frequency range of the ^{71}Ga nuclei in cross-peaks associated with a given ^{15}N frequency as one moves to larger Knight shifts, a spread which reaches its maximum of about 60 ppm (^{71}Ga) width in the asymmetric high-frequency tail of the distribution. *A priori* this spread could arise from three possible sources involving either chemical shifts, NQCCs, or Knight shifts. We rule out differential chemical shift changes of the two types of nuclei (e.g., from defects or surface effects) as the explanation, since Fig. 7 shows a good correlation between the ^{71}Ga and ^{15}N shifts (especially at larger shifts), as expected for a distribution arising solely from Knight shifts. We also rule out, on two grounds, NQCC effects due to Ga atoms in the direct vicinity of defects such as O_N substitutions (or N vacancies) having strongly asymmetric environments resulting in much larger ^{71}Ga quadrupolar interactions and associated spectral broadening (so-called second-order quadrupolar broadening). First, previous ^{71}Ga MAS NMR results on similar GaN nanoparticle materials found little or no evidence for anisotropic second-order quadrupolar

broadening effects across the Knight shift distribution [23]. Secondly, if such effects were responsible, then one would not expect Korringa-type relaxation behavior across the entire distribution of ^{71}Ga Knight shifts, as observed in Fig. 5(c).

We are led to conclude that each ^{15}N Knight shift isochromat is correlated with a distribution of ^{71}Ga Knight shifts whose width increases for the larger ^{15}N Knight shifts. To understand how this might happen, consider the inset to Fig. 6(a), which depicts a particular ^{15}N nucleus and the associated distances and calculated dipolar couplings to both a directly bonded ^{71}Ga nucleus as well as to next-nearest-neighbor ^{71}Ga nuclei. There are four closest sites for ^{71}Ga nuclei, and 24 sites for ^{71}Ga nuclei separated by a gallium and a nitrogen atom (having dipolar couplings to ^{15}N that are 19% or 8% of the directly bonded value). Thus, both directly bonded ^{71}Ga nuclei as well as next-nearest-neighbor ^{71}Ga nuclei will contribute to the observed signal intensity in the dipolar-coupling mediated $^{15}\text{N}\{^{71}\text{Ga}\}$ TEDOR spectrum shown in Fig. 6(a).

The increasing spread in the frequency range of the ^{71}Ga nuclei in cross-peaks associated with the most Knight-shifted ^{15}N nuclei can then be explained if those ^{15}N nuclei, such as depicted in the inset to Fig. 6(a), are close to the shallow donors, and thus experience the largest Knight shifts due to peaking of the electron wave function near donor sites [50]. Their four closest sites for ^{71}Ga nuclei, and their 24 sites for next-nearest-neighbor ^{71}Ga nuclei would then have significantly different nanoscale proximities to the same shallow donor, and hence different ^{71}Ga Knight shifts.

This interpretation in terms of varying local metallic properties is consistent with the larger ^{14}N Knight shifts associated with N atoms closer to (Ge) shallow donors in GaN:Ge [Fig. 1(b)]. A rough estimate of the magnitude of this spatial variation of ^{71}Ga Knight shifts can be made by assuming that the 60-ppm ^{71}Ga linewidth described above is due to a 60-ppm difference in Knight shifts between two ^{71}Ga nuclei attached to the same N atom with a 3.20-Å separation (from the crystal structure of hexagonal GaN), and with the internuclear vector aligned with the dopant atom for maximal effect. This yields a Knight shift spatial variation in the regions nearest the dopant of ca. 20 ppm/Å. The sensitivity of 2D NMR techniques to nanoscale variations of electronic structure thus provides a basis for spatially correlating the electronic properties of two atom types in compound semiconductors (bulk or nanocrystalline) doped above the MIT for comparison with theoretical calculations of such properties. The attribution of at least some part of the observed distribution of Knight shifts to nanoscale variations in electronic structure, based upon these experimental results, has significant implications. It indicates that interpreting observed Knight shift distributions in terms of macroscopic (rather than nanoscopic) probability distributions of carrier densities is not justifiable in the way originally proposed [14,18].

3. Likely shallow donors in nanocrystalline GaN

Oxygen substitution on an N site (O_N) is likely to be present in the nanocrystalline GaN materials, which were prepared from an oxygen-containing precursor, GaO(OH). The XRD pattern [Fig. 5(a)] of the nanocrystalline natural abundance

GaN shows weak reflections that are indexable to $\beta\text{-Ga}_2\text{O}_3$ (<3%), consistent with oxygen being present in the sample. This impurity is not visible in the ^{71}Ga NMR spectrum in Fig. 5(b) due to its dilute quantity and inhomogeneously broadened signals. Oxygen doping in GaN is usually associated with Ga vacancies (V_{Ga}), which act as triple acceptors and partially compensate the O_N shallow donors. Typically, V_{Ga} and O_N are assumed to form a complex which acts as a deep level, and only the uncompensated O_N will act as shallow donors [51]. Nitrogen vacancies could also be present, given that the synthesis temperature is high enough to dissociate GaN under vacuum [52]. However, nitrogen vacancies are reported to be energetically unfavorable under n-type conditions, with a formation energy that depends greatly on Fermi level [51].

The most energetically favorable shallow donors in n-type GaN are O_N , Si_{Ga} , and Ge_{Ga} [51], of which O_N is the most physically reasonable given the presence of oxygen in the starting material. The GaN wurtzite lattice can accommodate large concentrations of O atoms while maintaining tetrahedral coordination of Ga atoms [53]. However, Si_{Ga} cannot be totally ruled out since the ammonolysis was done in alumina crucibles, and typical alumina ceramics use silica-based sintering aids in their manufacture. A recent modeling study based on hybrid functional calculations [54] predicted similar shallow-donor electronic behaviors for O_N and Ge_{Ga} substitution defects in GaN, which is fully consistent with our analyses of the similar NMR spectral features and corresponding electronic structures observed here for nanocrystalline GaN and bulk GaN:Ge. These results are also consistent with previous results [23] for nanocrystalline GaN synthesized differently, which exhibited a broad distribution of Knight-shifted intensities [39].

III. CONCLUSIONS

In summary, ^{71}Ga , ^{14}N , and ^{15}N MAS-NMR experiments have provided detailed new insights on the similar local electronic structures of nanocrystalline and doped bulk GaN. They reveal the highly metallic character of both bulk GaN heavily doped n type with Ge and nanocrystalline GaN made by high temperature ammonolysis, and conclusively demonstrate the origin of the shifts observed in the latter material to be conduction band electrons. Such high carrier concentrations in nanocrystalline GaN are most likely due to oxygen atoms from the GaO(OH) precursor, which are known to give rise to n-type GaN in bulk [51,53].

Measurements of Korringa spin-lattice relaxation times for differing Knight shifts across the spectra prove that both forms of GaN are well above their MIT, with carriers exhibiting the near-ideal characteristics of a degenerate Fermi gas of noninteracting spins. This close approach to ideal behavior, which contrasts with deviations from ideal Korringa behavior often observed for true metals [55], can be attributed to the orders of magnitude lower carrier concentration in the degenerately doped semiconductor.

The magnitude and character of the conduction electron wave functions at the Group III and Group V nuclear sites have been previously measured in other bulk metallic semiconductors [56]. Here we have determined the Group V/III ratio of s-orbital carrier wave function probabilities at

the Fermi edge across the entire distribution of Knight shifts in both bulk-doped and nanocrystalline materials, with the N to Ga ratios equal to ca. 1.7 for both forms.

Two-dimensional $^{15}\text{N}\{^{71}\text{Ga}\}$ NMR results establish that the local metallic properties (Knight shifts) at Ga and N sites are spatially correlated on a subnanometer scale. They provide additional evidence that distributions of Knight shifts are due to electronic disorder arising from differing proximities to randomly located shallow donors. This conclusion supports a previous theoretical model accounting for ^{29}Si Knight shift distributions in doped silicon also based upon such proximities [9]. Such detailed insights on atomic-level electronic structures are expected to be relevant generally to Group III-V and other technologically important semiconducting solids. The present approach to observing spatial correlations in electronic structure between different atom types should thus prove valuable in future investigations of nanocrystalline semiconductors, where

the effects of interfaces and randomly substituted dopants on the MIT are not well understood, and in comparisons of their properties to those in doped bulk analogs.

ACKNOWLEDGMENTS

The authors acknowledge support from the Office of Naval Research and the U.S. National Science Foundation (Grant No. MSN-CHE-1059108). The TEM, XRD, and NMR measurements on the GaN nanoparticles were conducted using the Central Facilities of the UCSB Materials Research Laboratory, supported by the MRSEC Program of the NSF (Grant No. DMR-1121053), which is a member of the NSF-funded Materials Research Facilities Network (www.mrfln.org). The authors also thank J.D. Epping, U. Werner-Zwanziger, B. Dunlap, and K. Hoang for insightful discussions.

-
- [1] N. F. Mott, *Adv. Phys.* **21**, 785 (1972).
- [2] W. Kohn and J. M. Luttinger, *Phys. Rev.* **98**, 915 (1955).
- [3] E. B. Hale and R. L. Mieher, *Phys. Rev.* **184**, 739 (1969).
- [4] J. L. Ivey and R. L. Mieher, *Phys. Rev. B* **11**, 822 (1975).
- [5] J. L. Ivey and R. L. Mieher, *Phys. Rev. B* **11**, 849 (1975).
- [6] S. B. Orlinskii, J. Schmidt, E. J. J. Groenen, P. G. Baranov, C. de Mello Donega, and A. Meijerink, *Phys. Rev. Lett.* **94**, 097602 (2005).
- [7] D. Belitz and T. R. Kirkpatrick, *Rev. Mod. Phys.* **66**, 261 (1994).
- [8] W. Sasaki, I. Seiichiro, and S. Kobayashi, *J. Phys. Soc. Jpn.* **36**, 1377 (1974).
- [9] H. Kamimura, *Philos. Mag.* **29**, 65 (1974).
- [10] S. Kobayashi, Y. Fukagawa, S. Ikehata, and W. Sasaki, *J. Phys. Soc. Jpn.* **45**, 1276 (1978).
- [11] M. J. Hirsch and D. F. Holcomb, *Phys. Rev. B* **33**, 2520 (1986).
- [12] E. M. Meintjes, J. Danielson, and W. W. Warren, Jr., *Phys. Rev. B* **71**, 035114 (2005).
- [13] M. J. R. Hoch and D. F. Holcomb, *Phys. Rev. B* **71**, 035115 (2005).
- [14] J. P. Yesinowski, *Top. Curr. Chem.* **306**, 229 (2012).
- [15] U. K. Mishra, L. Shen, T. E. Kazior, and Y. F. Wu, *Proc. IEEE* **96**, 287 (2008).
- [16] S. P. DenBaars, D. Feezell, K. Kelchner, S. Pimpitkar, C. C. Pan, C. C. Yen, S. Tanaka, Y. Zhao, N. Pfaff, R. Farrell, M. Iza, S. Keller, U. K. Mishra, J. S. Speck, and S. Nakamura, *Acta Mater.* **61**, 945 (2013).
- [17] C. P. Slichter, *Principles of Magnetic Resonance*, 3rd ed. (Springer-Verlag, Berlin, 1990).
- [18] J. P. Yesinowski, A. P. Purdy, H. Q. Wu, M. G. Spencer, J. Hunting, and F. J. DiSalvo, *J. Am. Chem. Soc.* **128**, 4952 (2006).
- [19] The GaN:Ge sample was identical to the sample used in Ref. [18].
- [20] B. Schwenzer, J. Hu, R. Seshadri, S. Keller, S. P. DenBaars, and U. K. Mishra, *Chem. Mater.* **16**, 5088 (2004).
- [21] W. S. Jung and B. K. Min, *Mater. Lett.* **58**, 3058 (2004).
- [22] M. Drygas, Z. Olejniczak, E. Grzanka, M. M. Bucko, R. T. Paine, and J. F. Janik, *Chem. Mater.* **20**, 6816 (2008).
- [23] B. Schwenzer, J. Hu, and D. E. Morse, *Adv. Mater.* **23**, 2278 (2011).
- [24] W. S. Jung, *Ceram. Int.* **38**, 5741 (2012).
- [25] M. Drygas, M. Sitarz, and J. F. Janik, *RSC Adv.* **5**, 106128 (2015).
- [26] J. P. Yesinowski, *J. Magn. Reson.* **252**, 135 (2015).
- [27] J. P. Yesinowski and A. P. Purdy, *J. Am. Chem. Soc.* **126**, 9166 (2004).
- [28] E. M. Meintjes, W. W. Warren, Jr., and J. P. Yesinowski, *Solid State Nucl. Magn. Reson.* **55–56**, 91 (2013).
- [29] R. Minikayev, W. Paszkowicz, P. Piszora, M. Knapp, C. Bächtz, and S. Podsiadlo, *X-Ray Spectrom.* **44**, 382 (2015).
- [30] C. Persson, B. E. Sernelius, A. F. da Silva, R. Ahuja, and B. Johansson, *J. Phys.: Condens. Matter* **13**, 8915 (2001).
- [31] A. Wolos, Z. Wilamowski, M. Piersa, W. Strupinski, B. Lucznik, I. Grzegory, and S. Porowski, *Phys. Rev. B* **83**, 165206 (2011).
- [32] A. F. da Silva and C. Persson, *J. Appl. Phys.* **92**, 2550 (2002).
- [33] J. P. Yesinowski, *Phys. Status Solidi C - Conferences and Critical Reviews* **2**, 2399 (2005).
- [34] N. A. Mahadik, S. B. Qadri, M. V. Rao, and J. P. Yesinowski, *Appl. Phys. A* **86**, 67 (2007).
- [35] J. R. Morton and K. F. Preston, *J. Magn. Reson.* **30**, 577 (1978).
- [36] K. Lawniczak-Jablonska, T. Suski, I. Gorczyca, N. E. Christensen, K. E. Attenkofer, R. C. C. Perera, E. M. Gullikson, J. H. Underwood, D. L. Ederer, and Z. L. Weber, *Phys. Rev. B* **61**, 16623 (2000).
- [37] G. Denninger, R. Beerhalter, D. Reiser, K. Maier, J. Schneider, T. Detchprohm, and K. Hiramatsu, *Solid State Commun.* **99**, 347 (1996).
- [38] J. P. Yesinowski, *J. Magn. Reson.* **180**, 147 (2006).
- [39] See Supplemental Material at <http://link.aps.org/supplemental/10.1103/PhysRevB.95.235201> for additional experimental details and discussion.
- [40] M. Corti, A. Gabetta, M. Fanciulli, A. Svane, and N. E. Christensen, *Phys. Rev. B* **67**, 064416 (2003).
- [41] D. J. Norris, A. L. Efros, and S. C. Erwin, *Science* **319**, 1776 (2008).
- [42] X. Liu and M. T. Swihart, *Chem. Soc. Rev.* **43**, 3908 (2014).
- [43] A. W. Hing, S. Vega, and J. Schaefer, *J. Magn. Reson.* **96**, 205 (1992).
- [44] A. W. Hing, S. Vega, and J. Schaefer, *J. Magn. Reson., Ser. A* **103**, 151 (1993).

- [45] C. A. Fyfe, K. T. Mueller, H. Grondey, and K. C. Wong-Moon, *Chem. Phys. Lett.* **199**, 198 (1992).
- [46] C. A. Fyfe, K. T. Mueller, H. Grondey, and K. C. Wong-Moon, *J. Phys. Chem.* **97**, 13484 (1993).
- [47] E. R. H. Vaneck and W. S. Veeman, *J. Am. Chem. Soc.* **115**, 1168 (1993).
- [48] E. R. H. Vaneck and W. S. Veeman, *Solid State Nucl. Magn. Reson.* **2**, 307 (1993).
- [49] J. P. Amoureux, J. Trébosc, and G. Tricot, *Magn. Reson. Chem.* **45**, S187 (2007).
- [50] J. R. Meyer, F. J. Bartoli, and N. F. Mott, *Philos. Mag. B* **52**, L51 (1985).
- [51] C. G. Van de Walle and J. Neugebauer, *J. Appl. Phys.* **95**, 3851 (2004).
- [52] J. Unland, B. Onderka, A. Davydov, and R. Schmid-Fetzer, *J. Cryst. Growth* **256**, 33 (2003).
- [53] K. C. Mishra, P. C. Schmidt, S. Laubach, and K. H. Johnson, *Phys. Rev. B* **76**, 035127 (2007).
- [54] L. Gordon, J. L. Lyons, A. Janotti, and C. G. Van de Walle, *Phys. Rev. B* **89**, 085204 (2014).
- [55] J. Winter, *Magnetic Resonance in Metals*, The International Series of Monographs on Physics (Clarendon Press, Oxford, 1971).
- [56] D. P. Tunstall, *J. Phys. C: Solid State Phys.* **21**, 2853 (1988).

SUPPLEMENTAL MATERIAL

Spatially Correlated Distributions of Local Metallic Properties in Bulk and Nanocrystalline GaN

James P. Yesinowski,^{1*} Zachariah J. Berkson,² Sylvian Cadars,³ Andrew P. Purdy,¹ Bradley F. Chmelka²

1. Chemistry Division, Naval Research Laboratory Washington DC 20375-5342

2. Department of Chemical Engineering, University of California, Santa Barbara California 93106-5080

3. Institut des Matériaux Jean Rouxel (IMN), Université de Nantes, CNRS, BP32229, 44322 Nantes Cedex 3, France

Materials Synthesis

Nanocrystalline gallium nitride was synthesized by ammonolysis of micron-sized gallium oxide hydroxide (GaO(OH)) particles as previously reported [1]. Micron-sized GaO(OH) particles were prepared by placing 60 mL of 0.1 M aqueous gallium nitrate solution in a sealed container containing an excess amount (200 mL) of 1.2% NH₄OH solution. The gallium nitrate solution was stirred rapidly with a magnetic stir bar and allowed to react with the ammonia-containing atmosphere for 18 hours, after which the resulting white precipitate was collected by vacuum filtration, washed with deionized water, and dried under air. The product was identified as crystalline GaO(OH) by powder X-ray diffraction, with some amorphous component seen in the TEM, and characterized by ⁷¹Ga MAS-NMR (Fig. S1).

To prepare nanocrystalline GaN, the as-synthesized GaO(OH) powder was crushed to a powder, placed in an alumina crucible, and loaded into a quartz Schlenk tube. The tube was placed in a tube furnace and purged with nitrogen for 30 minutes prior to heating. The tube furnace was ramped to 750 °C at a rate of 15 °C/min under a flow of nitrogen gas. The nitrogen flow was turned off and was replaced by an ammonia flow of 20 standard cm³/min. For the synthesis of ¹⁵N-enriched nanocrystalline GaN, ammonia enriched to 99.9% in ¹⁵N was used. The tube furnace was then ramped to the annealing temperature of 1100 °C. The reaction was allowed to proceed for 2 hours, after which the tube was cooled to room temperature under continued ammonia flow. The resultant light yellow GaN powders were stored in sealed vessels in a vacuum desiccator to prevent degradation due to hydrolysis or oxidation.

The bulk Ge-doped GaN sample was synthesized by a Na/K flux method and characterized as described previously [2].

Materials characterization

The powder XRD measurements on the nanocrystalline GaN were conducted at room temperature on a Rigaku SmartLab High Resolution X-Ray Diffractometer or a Panalytical

Empyrean Powder X-Ray Diffractometer in θ - 2θ mode using Cu $K\alpha$ radiation with a wavelength of 1.54 Å. TEM micrographs were acquired using an FEI Tecnai G2 Sphera microscope with an acceleration beam voltage of 200 kV and a Gatan UltraScan 1000P CCD camera for image recording. Nanocrystalline GaN was prepared for TEM measurements by dispersing 1 mg of the powdered sample in 1 mL of dry methanol, sonicating for 10 – 15 minutes, and dispensing one to two drops of the suspension on a lacey carbon TEM grid.

Experimental: MAS-NMR measurements

GaN:Ge

For bulk Ge-doped GaN, ^{71}Ga (152.5 MHz) saturation-recovery data and the ^{14}N (36.1 MHz) Hahn echo spectrum in Fig. 1(b) were obtained on a Varian/Agilent DDPS 11.7 T NMR spectrometer using a variable-temperature 4.0 mm triple-resonance probe. The 90° pulse length for the central transition of ^{71}Ga was 1.7 μs , and for the non-selective ^{14}N transitions 10 μs . Chemical shifts for both nuclei were referenced to a 1M $\text{Ga}(\text{NO}_3)_3$ aqueous solution at zero ppm. A spectral width of 250 kHz (1.25 MHz) with 12800 (64000) data points were used for the ^{71}Ga , and ^{14}N spectra respectively. The ^{14}N spectrum was obtained with a rotor-synchronized $\pi/2$ - τ - π -Acquire Hahn echo pulse sequence with the delay between the midpoint of the pulses set to 83.3 μs , the inverse of the 12 kHz MAS rate; the data were Fourier-transformed after shifting to the echo maximum. Both central and satellite ^{71}Ga transitions were saturated by applying a train of sixty 1.7 μs pulses at 74 kHz from the central transition frequency spaced 2016 μs apart and thus asynchronous with the 200 μs rotor period. An asynchronous saturation pulse train has been shown to yield more reliable T_1 values than alternative methods [3]. An array of 30 saturation-recovery delay times was used with 64 scans for each delay, with a recycle delay of 0.5 s. The saturation-recovery curves were fit in MATLAB to a single exponential recovery from zero. At the shortest recovery time (3.3 ms) the signal intensity at the Knight shift maximum was only about 2% of the fully-recovered intensity, consistent with good saturation of the transition, and the measured T_1 for the maximal intensity Knight-shifted peak at 295 K of 0.497 ± 0.003 s agrees well with the corresponding carefully-determined “true T_1 ” in the same sample at 294 K of 0.491 ± 0.001 s [3].

The analyses shown in Fig. 3 are obtained after subtracting the $T_{1,0}^{-1}$ relaxation rate of the ^{71}Ga zero Knight shift peak measured at the different temperatures. The initial procedure to measure $T_{1,0}^{-1}$ was to measure the peak heights at the zero-Knight shift position relative to an extrapolated sloping baseline on either side of the peak, and to fit the heights to a biexponential saturation-recovery curve, yielding long and short T_1 components. The contribution from the short T_1 component (at 173 K, 295 K, and 473 K) varied from only 10 to 23% across the temperature range studied, so the values of the long T_1 component (5.86 s, 2.07 s and 0.80 s at the respective temperatures) represent the dominant relaxation behavior. Constraining the fraction of the short T_1 component to be 12.8 % (the average value from fits at all six temperatures) yielded similar long T_1 component values of 6.47 s, 2.06 s and 0.68 s at the respective temperatures. To have a standard means of obtaining the zero Knight shift relaxation rate for the analyses in Fig. 3, we fit the recovery data to a single exponential function, yielding values and error bars of 4.4 (0.5) s, 1.8 (0.1) s, and 0.7 (0.1) s. (If we use the longer T_1 values at 173 K obtained from either biexponential analysis, the deviations in Fig. 3(b) seen for 173 K data at $K < 70$ ppm and $K > 200$ ppm become even more pronounced.) We note that the T_1 value at

295 K is somewhat shorter than either that measured in an undoped wurtzite GaN sample at 304 K (=3.51 s)[4] or the extrapolation of that value to one at 295 K (= 3.76 s) assuming a previously-observed T^3 dependence of the relaxation rate due to the quadrupolar mechanism [5].

The ^{14}N (36.13 MHz) saturation-recovery T_1 measurements of Ge-doped GaN at 11.7 T analyzed in Fig. 4 were carried out on a Bruker DMX-500 spectrometer with a $^1\text{H}/^{14}\text{N}$ double-resonance insert on a 4.0 mm triple-resonance probe, having a (non-selective) $\pi/2$ pulse length of 8.5 μs . The spinning speed was 9.0 kHz, with a train of six $\pi/2$ saturating pulses followed by a rotor-synchronized $\pi/2$ - τ - π -Acquire Hahn echo pulse sequence as described above. The saturation-recovery intensities at each centerband frequency were fit to a single exponential T_1 . Neglecting the spinning sidebands in the T_1 analysis, which contribute to the “complete” ^{14}N spectrum as indicated in the inset to Fig. 1(b), is justifiable on the following grounds. Although the centerband peak does not represent equally all crystallite orientations, favoring those whose principal axis of the axially-symmetric ^{14}N NQCC tensor are aligned near the rotor axis and hence unmodulated by MAS, the Knight shift (Fermi contact) interaction is isotropic. Thus, Eq. 2 is expected to apply regardless of which subset of crystallite orientations is investigated.

A recycle delay of 20 s was used to acquire 12056 scans (67 h) for the ^{14}N MAS-NMR spectrum of Fig. 1(b). Based on the measured T_1 values, this results in a partial saturation of the weak sharp zero Knight shift peak (3.0 ppm FWHM) as well as that portion of the spectrum with small Knight shifts. The smaller ^{14}N relative to ^{71}Ga intensity seen in this region in Fig. 1(c) is attributed to this partial saturation effect. In Fig. 1(b) the symmetrically situated peaks on either side of the centerbands of both the zero Knight shift peak and that of the Knight shift distribution are spinning sidebands arising primarily from the ^{14}N NQCC (= $e2Qq/h$), which in undoped GaN is 24.14 kHz [6]. A line-broadening apodization of 36 Hz (1.0 ppm) was used. The method of summing centerband and sidebands in Fig. 1(c) is essentially that of two-dimensional one-pulse (TOP) NMR [7], in the present case obtained by summing offset sections of the total spectra having spectral widths of the MAS rate.

Nanocrystalline GaN

The ^{71}Ga and ^{15}N MAS NMR measurements of the nanocrystalline GaN samples were performed on a Bruker AVANCE-III Ultrashield Plus 800 MHz (18.8 T) narrow-bore spectrometer operating at Larmor frequencies of 244.1 and 81.1 MHz for ^{71}Ga and ^{15}N , respectively, and using a Bruker 3.2 mm broadband Bruker Tri-Gamma H-X-Y probehead. The ^{71}Ga shifts were referenced to a 0.1 M gallium nitrate solution at 0.0 ppm. In order to provide a comparison to the ^{14}N shifts in GaN:Ge referenced to a 1M gallium nitrate, the ^{15}N shifts were measured against ^{15}N -labeled glycine but then adjusted to the ^{15}N shift of a 1M aqueous nitrate solution.

The ^{71}Ga spin-lattice (T_1) relaxation times of the nanocrystalline GaN sample were measured by using a saturation recovery pulse sequence with a rotor-asynchronous saturating pulse train with a ^{71}Ga $\pi/2$ pulse of 1.3 μs [3]. The solid-state 2D $^{15}\text{N}\{^{71}\text{Ga}\}$ transferred-echo double resonance (TEDOR) spectrum of nanocrystalline Ga ^{15}N was acquired using a π pulse length of 10 μs on ^{71}Ga to reintroduce the heteronuclear ^{15}N - ^{71}Ga dipolar couplings. To maximize signal intensity in the direct dimension, the spectrum was acquired using the Carr-

Purcell-Meiboom-Gill (CPMG) acquisition method [8], by generating and acquiring series of echoes, accumulating the signal of all these echoes and co-adding for each transient. Signal enhancement is only obtained in favorable cases where the spectrum is broad relative to the inverse of the lifetime of transverse coherences (*i.e.* where the inhomogeneous linewidth is much larger than the homogeneous one). This is typically the case for ^{15}N nuclei in the nanocrystalline Ga^{15}N , since the width of the one-dimensional ^{15}N spectrum is on the order of 10^2 ppm (*i.e.*, 8×10^3 Hz at 18.8 T) due to Knight shift distributions while the inverse transverse dephasing times measured here are on the order of 1 Hz. For each scan, 320 echoes were collected during the acquisition for a total acquisition time of 0.55 seconds. This yields a signal intensity increase by a factor of ca. 18 as compared to a spectrum collected without CPMG acquisition. Furthermore, in this experiment, the fast-relaxing ^{71}Ga nucleus is excited first and then transfers its magnetization to nearby ^{15}N nuclei using the TEDOR pulse sequence, which means that experiments can be repeated rapidly. As most of the ^{71}Ga magnetization is recovered during the 0.55 s during which the ^{15}N signal is collected, the experiment can be repeated immediately, and thus the recycle delay was set to 1 ms.

Supplemental Discussion and Analysis

Lack of significant eddy-current heating effect from MAS of GaN:Ge conductive sample

We note that the good agreement of the data points in Fig. 4(a) to the dashed line representing Eq. (2) is a good indication that the sample is at a temperature close to that measured by the nearby thermocouple, and not significantly heated by induced currents generated by rotating a conductive sample in a magnetic field as has been seen for $\gamma\text{-CuI}$. [9]. Further confirmation of the lack of a significant heating effect from induced currents, which varies quadratically with spinning speed [9], is the unchanged T_1 measured when the spinning speed was increased to 12 kHz.

Analyses of Korringa relaxation times $T_{1,K}$ at different magnetic field strengths

In general, experimental results agree very well with Eq.(2) for both the bulk GaN:Ge and nanocrystalline GaN materials despite the difference in experimental magnetic field strengths (11.7 T and 18.8 T, respectively). This is fully consistent with the expected field-independence of the Korringa relaxation mechanism described by Eq.(2).

^{14}N MAS-NMR

In the ^{14}N MAS-NMR spectrum of undoped GaN, one centerband peak was observed with a chemical shift of -301.8 ppm with respect to 1 M $\text{Ga}(\text{NO}_3)_3$ [10] and a very long T_1 of 591 s [11]. The present observation of a broad ^{14}N MAS-NMR spectrum due to a Knight shift distribution is consistent with similar results for a Mn,Ge-doped GaN sample that had been co-doped with Ge in order to increase the concentration of Mn^{2+} [12]. The T_1 of the zero Knight shift peak is 38.5 s, considerably shorter than the 591 s value in the undoped GaN sample [11]. An analogous reduction was seen in the ^{71}Ga T_1 values discussed above.

Calculation of $^{71}\text{Ga} / ^{15}\text{N}$ dipolar couplings

Both ^{71}Ga to ^{15}N distances and calculated $^{71}\text{Ga} / ^{15}\text{N}$ dipole-dipole couplings are shown schematically in the inset to Fig. 6(a). The dipole couplings between two nuclei, b_{12} , were calculated by:

$$b_{12} = -\frac{\mu_0 \gamma_{n1} \gamma_{n2} \hbar}{8\pi^2 r^3}$$

where μ_0 is the permeability of free space, γ_{n1} and γ_{n2} are the nuclear gyromagnetic ratios of ^{71}Ga and ^{15}N , respectively, \hbar is Planck's constant, and r is the distance between the two nuclei.

Comparison to previous ^{71}Ga NMR results reported for nanocrystalline GaN

Previous work [1] involving nanocrystalline GaN prepared by ammonolysis of GaO(OH) at 1100 °C is consistent with the results reported in Section II.B. The ^{71}Ga NMR spectrum in that study showed a broad peak with approximately the same ^{71}Ga Knight shift distribution as observed for our nanocrystalline samples, although the small impurity Ga₂O₃ reflections in the XRD pattern were not observed. In the previous work [1], the materials were reported to contain oxygen and to be highly N-deficient based on energy dispersive spectroscopy (EDS), though we note that the EDS method of elemental analysis is subject to large systematic errors and is unreliable without careful calibration standards. Nevertheless, the presence of oxygen is consistent with our discussion in Section II.B.3 regarding the possibility of oxygen atoms as shallow donors in the annealed nanocrystalline GaN.

Supplemental Figures

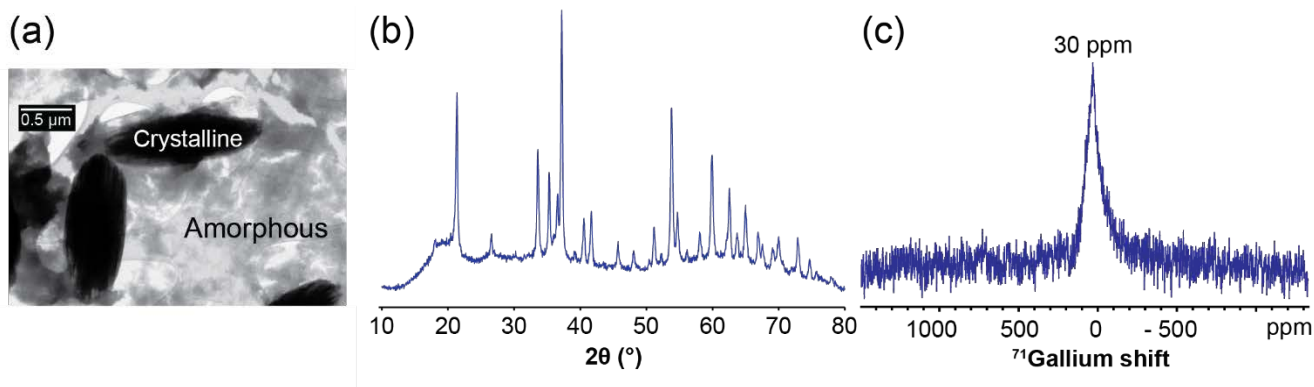


Figure S1. Characterization of the GaO(OH) material used as a precursor to the natural abundance GaN nanoparticles: (a) Representative transmission electron micrograph image showing the presence of microcrystalline and amorphous GaO(OH), (b) Powder X-ray diffraction pattern, and (c) Solid-state 1D ^{71}Ga MAS NMR spectrum (18.8 K, 5 kHz spinning, 298 K, 2 s recycle delay) showing a single broad peak at 30 ppm.

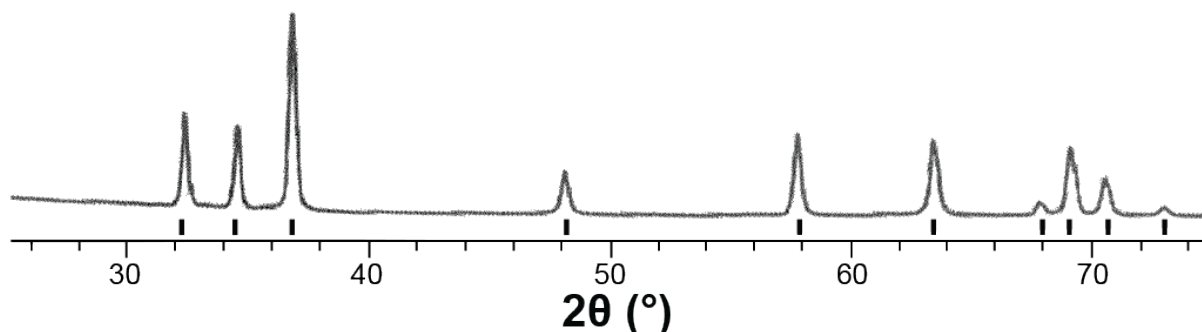


Figure S2. Powder X-ray diffraction pattern of nanocrystalline GaN synthesized by annealing GaO(OH) at 1100 °C with NH₃ isotopically-enriched to 99.9% abundance of ¹⁵N; the black lines indicate reflections indexable to wurtzite GaN (JCPDS Card No. 76-073).

References

- [1] B. Schwenzer, J. Hu, and D. E. Morse, *Advanced Materials* **23**, 2278 (2011).
- [2] J. P. Yesinowski, A. P. Purdy, H. Q. Wu, M. G. Spencer, J. Hunting, and F. J. DiSalvo, *J. Am. Chem. Soc.* **128**, 4952 (2006).
- [3] J. P. Yesinowski, *J. Magn. Reson.* **252**, 135 (2015).
- [4] J. P. Yesinowski, *Journal of Magnetic Resonance* **180**, 147 (2006).
- [5] M. Corti, A. Gabetta, M. Fanciulli, A. Svane, and N. Christensen, *Physical Review B* **67**, 064416 (2003).
- [6] J. P. Yesinowski, *physica status solidi (c)* **2**, 2399 (2005).
- [7] B. Blumich, P. Blumler, and J. Jansen, *Solid State Nucl. Magn. Reson.* **1**, 111 (1992).
- [8] I. Hung, A. J. Rossini, and R. W. Schurko, *Journal of Physical Chemistry A* **108**, 7112 (2004).
- [9] J. P. Yesinowski, H. D. Ladouceur, A. P. Purdy, and J. B. Miller, *J. Chem. Phys.* **133**, 234509 (2010).
- [10] J. P. Yesinowski and A. P. Purdy, *J. Am. Chem. Soc.* **126**, 9166 (2004).
- [11] J. P. Yesinowski, *Topics in Current Chemistry* **306** 229 (2012).
- [12] A. P. Purdy, J. P. Yesinowski, and A. T. Hanbicki, *physica status solidi (c)* **2**, 2437 (2005).